

STREAMLINING THE IMAGE STITCHING PIPELINE: INTEGRATING FUSION AND RECTANGLING INTO A UNIFIED MODEL

A PREPRINT

 Ziqi Xie*

College of Electronics and Information Engineering
Tongji University, Siping Street, Shanghai, 201804, China
xieziqi@tongji.edu.cn

April 24, 2024

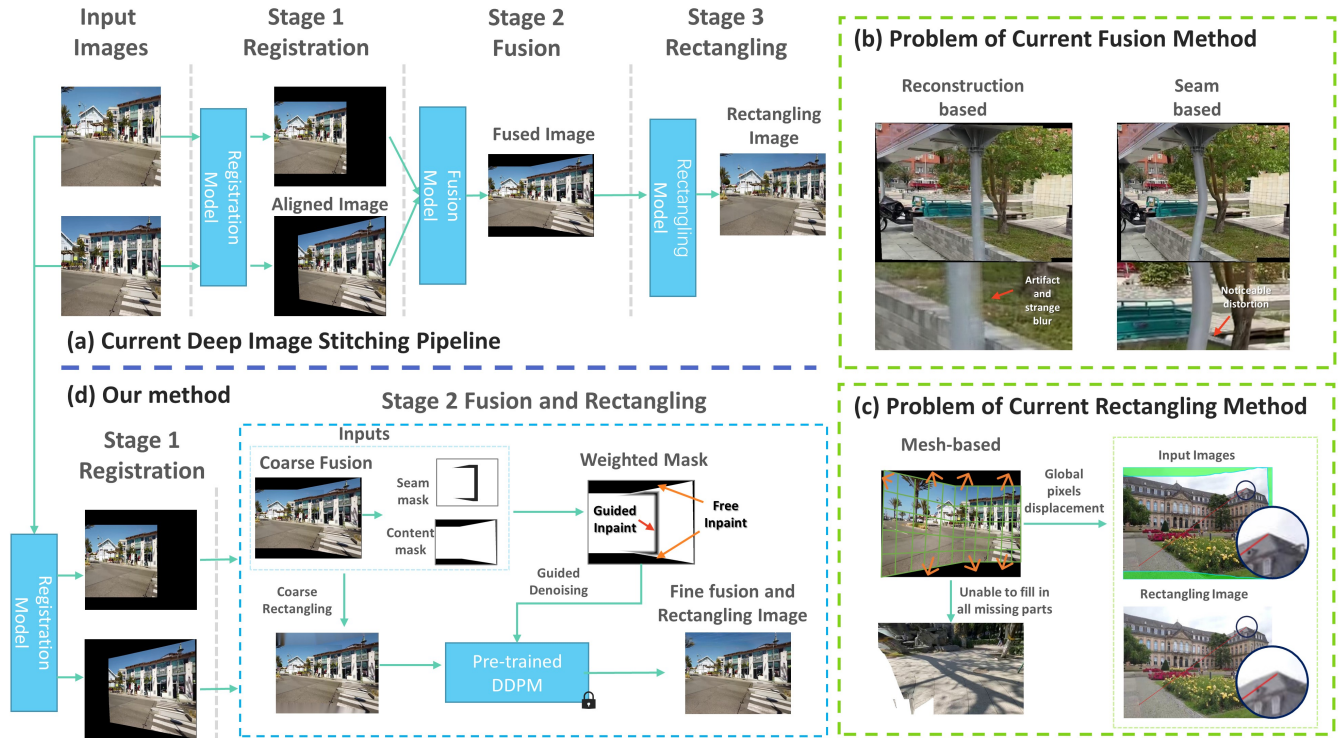


Figure 1: **Comparison between existing method and our method.** (a) Current learnig-based image stitching pipeline. (b) Problems with the current fusion method, reconstruction-based image is obtained by UDISNie et al. [2021], and seam-based image is obtained by UDIS++Cheng et al. [2023]. (c) Problems with the current rectangling method, obtained by Rectangling[Nie et al., 2022]. (d) Our method, a coarse-to-fine process. Coarse fusion overlaps two images without complex computations, and coarse rectangling employs straightforward interpolation to fill in missing areas. Then, a weighted mask directs a pre-trained DDIP model to refine the coarse input into the final image. This method effectively leverages the strengths of the large-scale pre-trained model without the need for additional fine-tuning.

*Use footnote for providing further information about author (webpage, alternative address)—*not* for acknowledging funding agencies.

ABSTRACT

Learning-based image stitching techniques typically involve three distinct stages: registration, fusion, and rectangling. These stages are often performed sequentially, each trained independently, leading to potential cascading error propagation and complex parameter tuning challenges. In rethinking the mathematical modeling of the fusion and rectangling stages, we discovered that these processes can be effectively combined into a single, variety-intensity inpainting problem. Therefore, we propose the Simple and Robust Stitcher (SRStitcher), an efficient training-free image stitching method that merges the fusion and rectangling stages into a unified model. By employing the weighted mask and large-scale generative model, SRStitcher can solve the fusion and rectangling problems in a single inference, without additional training or fine-tuning of other models. Our method not only simplifies the stitching pipeline but also enhances fault tolerance towards misregistration errors. Extensive experiments demonstrate that SRStitcher outperforms state-of-the-art (SOTA) methods in both quantitative assessments and qualitative evaluations. The code is released at <https://github.com/yayoyo66/SRStitcher>

Keywords Image Stitching · Image Fusion · Image Rectangling · Diffusion Model

1 Introduction

Image stitching is a fundamental problem in computer vision, which aims to obtain a larger field of view by merging multiple overlapping images. Typically, the image stitching pipeline comprises three distinct stages, as depicted in Figure 1(a)):

- Registration stage: This stage involves estimating warping matrices, such as homography, between input images and aligning these images based on the estimated results.
- Fusion stage: Subsequently, this stage merges the aligned images into a single fusion image.
- Rectangling stage: Finally, this stage transforms the irregularly shaped stitched image into a standard rectangular format.

Annoyingly, the sequential dependency of these stages introduces a significant limitation: next stage cannot start until the previous stage is totally completed. This cascading structure not only increases the likelihood of error propagation through the stages but also complicates the optimization of parameters, presenting substantial challenges in both the training and application of the image stitching pipeline.

Additionally, there are also some inherent issues in current stitching pipeline:

Fusion Stage Issues: the two current mainstream methods, reconstruction-based Nie et al. [2021] and seam-based Cheng et al. [2023], are prone to notable inaccuracies when dealing with misregistration errors between aligned images. These errors are evident in Figure 1(b), where even subtle misalignments can lead to noticeable errors in the stitched output, undermining the visual integrity of the resulting image.

Rectangling Stage Issues: Current methods are mainly mesh-based [Nie et al., 2022], which can introduce global pixel position distortions. This often results in notable image distortions, particularly in challenging scenarios. As illustrated in Figure 1(c), when comparing images pre and post-rectangling, a marked misalignment is observed. For example, a red line drawn between two points on the input image can not align with the corresponding points on the rectangling image, indicating a shift in the target point (the roof line is not aligned). This issue is critical as stitched images are often used for subsequent high-level vision tasks, where such subtle inter-pixel shifts can detrimentally affect the results of those tasks.

Given the above limitations observed in current stitching methods, particularly in terms of cascading errors and inefficiencies in the fusion and rectangling stages, we have reconsidered the underlying structure of the image stitching pipeline. Previous image stitching works [Nie et al., 2020a, 2021, 2022, 2023] typically address fusion and rectangling as distinct processes. However, our comprehensive analysis raises a critical question: *Are these really separate challenges?*

The primary objective of the fusion stage is to seamlessly integrate aligned images, specifically targeting and modifying discrepancies at their overlap. Conversely, the rectangling stage aims to transform an irregularly shaped composite into a regular rectangle, essentially filling in the missing image area. On closer inspection, both tasks—modifying and filling—can fundamentally be perceived as variations of an *inpainting problem* (refer to 7.2 for a detailed proof). While fusion requires adjusting the original image information in the overlapping areas, rectangling focuses on aesthetic consistency and coherence with adjacent areas.

This insight led us to propose a novel paradigm: a unified inpainting-based approach that addresses both fusion and rectangling simultaneously. We introduce SRStitcher, which simplifies the complex image stitching pipeline into a more elegant implementation. Our method demonstrates exceptional error tolerance, ensuring robust results even with less-than-ideal registration of images. Additionally, SRStitcher effectively addresses the issue of global pixel displacement inherent in previous rectangling methods, by selectively modifying and filling parts of the image without extensive pixel shifts. The contributions of this paper are summarized as follows:

- We re-think the fusion and rectangling tasks of existing image stitching pipelines. Through theoretical analysis, we demonstrate that both can be effectively addressed as a unified inpainting problem, leading to a more streamlined and robust pipeline.
- By using a pre-trained large-scale model, SRStitcher innovatively tackles both fusion and rectangling simultaneously. This method leverages the model’s strong generalization capabilities, utilizing weighted masks to guide the inpainting process across different image regions. Our method significantly reduces training time and hardware requirements, eliminating the need for model training or fine-tuning.
- We conduct extensive experiments on public dataset, employing state-of-the-art metrics including no-reference image quality assessment and user study to evaluate SRStitcher’s performance.

2 Related Work

The image stitching pipeline can be divided into three stages, and the related works are described based on each stage.

2.1 Image Registration

Early image registration works[Zoghlami et al., 1997, Capel and Zisserman, 1998, McLauchlan and Jaenicke, 2002] are limited by the feature extraction method, which often falter under conditions of rotation, scaling, and illumination changes. To solve the scale changes problem, AutoStitch[Brown and Lowe, 2007] marked a significant advancement by incorporating the Scale-invariant Feature Transform (SIFT) to extract scale-invariant features, but this method is difficult to apply to the situation with multiple depth layers. To specifically address multi-depth layers condition, DHW[Gao et al., 2011] proposed a model that assumes the presence of two distinct planes within the image, applying different homography adjustments to each. However, the performance of this method can be severely impacted by the dynamics of camera movement. More recently, NIS[Liao and Li, 2023] introduced depth map integration to enhance registration accuracy. However, this method relies on accurate estimation of depth maps, which presents its own set of implementation challenges. Yu et al.[Yu et al., 2023] developed a technique using the Epipolar Displacement Field, aimed at improving registration in scenes with significant parallax.

Feature-based methods have traditionally been the cornerstone of image registration techniques. However, these methods often underperform in environments without sufficient geometric structure or in low-texture scenarios where traditional feature detection techniques are prone to failure.

In recent years, the advent of deep learning has revolutionized the field of image registration by enabling the extraction of rich semantic features through deep neural networks. Hoang et al.[Hoang et al., 2020] and Shi et al.[Shi et al., 2020] both pioneered the use of Convolutional Neural Networks (CNNs) to enhance feature representations in image stitching registration. Despite their progress, these approaches primarily used deep learning for feature enhancement rather than creating a holistic learning-based framework. VFISNet[Nie et al., 2020b] is the first complete learning-based framework for image stitching, but it is limited by its inability to handle images of arbitrary resolutions. EPISNet[Nie et al., 2020a] is improved on VFISNet by introducing a flexible mechanism that supports the input of any image size through scalable image and homography adjustments. HomoGAN[Hong et al., 2022] introduces a method based on the Generative Adversarial Network(GAN) to enhance the quality of homography estimations, representing a novel application of GANs in this field. Jiang et al.[Jiang et al., 2023a] integrates graph convolutional networks into the image stitching framework to boost the precision of multi-spectral image registration. LBHomo[Jiang et al., 2023b] introduces a semi-supervised approach to estimate homography more accurately in large-baseline scenes by sequentially multiplying multiple intermediate homographies. RHWF[Cao et al., 2023] introduces homography guided image warping and Focus transformer into the recursive homography estimation framework to further refine homography estimation accuracy.

2.2 Image Fusion

The earliest fusion method is weighted fusion[Andrew, 2001], which requires high registration accuracy. If registration is imperfect or there is a color mismatch between the images, visible seams may appear, which can degrade image quality. APAP[Zaragoza et al., 2013] introduces a smoothly varying projection field to enhance fusion accuracy. However,

APAP tends to introduce severe perspective distortions in non-overlapping areas, limiting its applicability. Inspired by interactive digital photomontage [Agarwala et al., 2004], Gao et al. [Gao et al., 2013] proposed the seam-based fusion method, which involves a seam prediction stage to identify optimal seam lines between overlapping images. Although effective, it is notably time-consuming. Therefore, SEAGULL [Lin et al., 2016] proposes to improve the previous seam-based methods by using estimated seams to guide local alignment optimization, enhancing seam quality and reducing processing time. However, it struggles with repetitive textures, where it still shows poor performance.

The aforementioned methods are all traditional fusion methods, characterized by limited versatility and difficulty in adapting to complex scenarios. In order to solve the defects of traditional solutions, UDIS [Nie et al., 2021] proposed a reconstruction-based model to improve the quality of the fused image. Despite its advances, this method sometimes produces artifacts and strange blurs in overlapping areas. Inspiration from traditional seam-based approaches, UDS++ [Nie et al., 2023] and DseamCheng et al. [2023] both use deep learning to refine the seam finding process. These models offer more robust and flexible solutions, significantly improving the ability to handle complex stitching scenarios.

2.2.1 Image Rectangling

Image rectangling is a relatively new area of computer vision with limited research to date. Prior to the advent of deep learning in this domain, traditional solutions such as those proposed by He et al. [He et al., 2013] and Li et al. [Li et al., 2015] used mesh-based warping techniques to address missing areas in images. DeepRectangling [Nie et al., 2022] represents the first deep learning-based approach in image rectangling, accompanied by a baseline and a public dataset tailored for this specific task. The method continues to rely on mesh-based warping but incorporates learning algorithms to enhance the fill quality and handle complex scenarios more effectively. While these methods are groundbreaking, they often change the global relative pixel positions, which could lead to suboptimal results, especially in cases with large missing areas, resulting in incomplete fills. A more recent method RecDiffusion [Zhou et al., 2024] that employs a diffusion model to better solve the problem of rectangling. Although this method provides a sophisticated solution for achieving rectangularity, it is complex in design, requires long inference times, and requires significant computational resources for training, which limits its practical applicability.

3 Method

The architecture of StitchDiffer is depicted in Figure 1(d), which integrates the tasks of fusion and rectangling into a unified challenge of composite image inpainting. The StitchDiffer pipeline accepts as input two images with overlapping regions, designated as $I_l(x, y)$ and $I_r(x, y)$, where x and y represent the pixel coordinates. The specific design details are introduced below.

3.1 Registration

The registration stage is not the primary focus of this paper, we employ a simplified homography estimation network from UDIS++ [Nie et al., 2023] to address the registration challenges. It is important to clarify that this does not imply a devaluation of the registration stage. In fact, registration has been the most extensively researched of the three stitching stages, with significant work devoted to improving homography accuracy [Hong et al., 2022, Jiang et al., 2023b, Cao et al., 2023]. However, perfect homography matrices that precisely align images do not exist for scenes that are non-planar or that involve cameras with different centers of projection.

To overcome these inherent limitations, two mainstream methods have been identified: the multi-homography warp method [Zaragoza et al., 2013] and the dense match method [Truong et al., 2020]. However, the multi-homography method faces challenges in parallelization and integration within deep learning frameworks [Nie et al., 2023], while dense matching is generally slower and less robust.

These limitations inform our decision to use a straightforward homography network. This choice allows us to focus on improving the fault tolerance of the fusion stage through the powerful generalization capabilities of a large-scale generative model. As a result, our approach can produce visually appealing fusion results even with less precise registration. This strategy is a departure from previous image stitching work that has focused primarily on registration accuracy.

In summary, in the registration stage, we introduce UDIS++’s homography estimation method to calculate the homography between the input images $I_l(x, y)$ and $I_r(x, y)$. This homography maps the images onto a unified plane, resulting in aligned images $I_{wl}(x, y)$ and $I_{wr}(x, y)$, along with their corresponding masks $M_{wl}(x, y)$ and $M_{wr}(x, y)$.

3.2 Fusion and Rectangling

In designing the fusion and rectangling stages, we conceptualize the fusion and rectangling tasks as facets of a unified composite inpainting challenge. This approach relies on differentiating the inpainting requirements between the two stages: the fusion stage requires content-aware conditional inpainting to ensure seamless integration, while the rectangling stage allows for more flexible inpainting. As shown in Figure 2, our method differs from traditional fusion techniques by implementing a coarse-to-fine process. First, we use coarse fusion and rectangling techniques based on established image processing methods to obtain the coarse fusion image. We then refine the output by inpainting using large-scale diffusion models.

Our method employs a coarse-to-fine process to ensure semantic consistency in the output image and to prevent the inclusion of unwanted elements, such as illegible text or anomalous textures. In fact, our method requires only minor adaptations to perform both fusion and rectangling stages, without an initial coarse rectangling stage (more details are provided in the 7.5). However, omitting the coarse rectangling step can lead to semantically unstable images. Therefore, we advocate a coarse-to-fine processing scheme to address this issue.

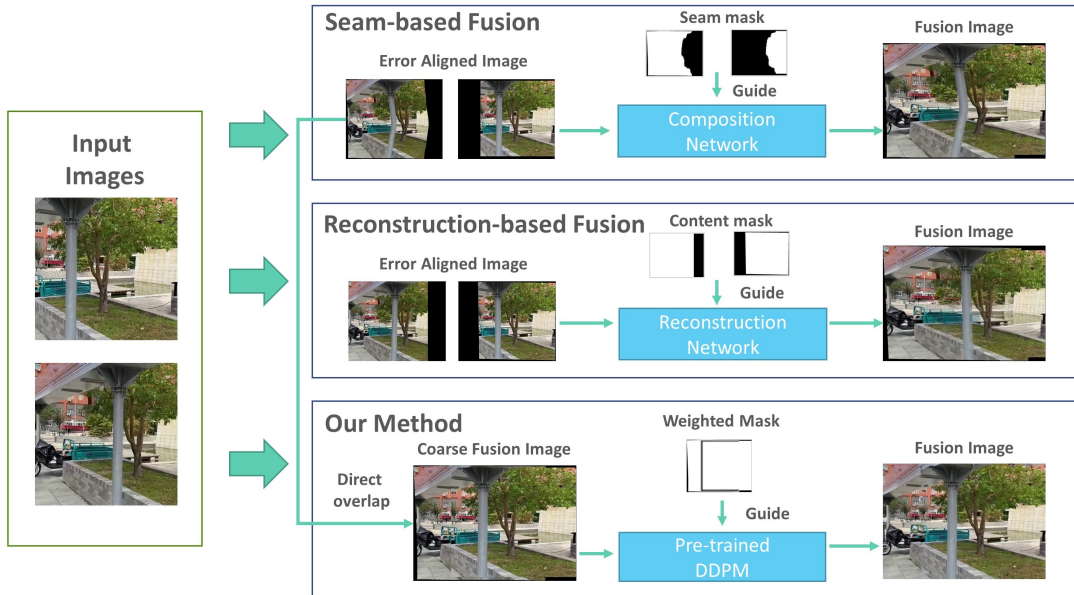


Figure 2: **Differentiating our method from existing fusion techniques.** Our method demonstrates enhanced robustness, particularly in scenarios where registration errors are present. In the coarse fusion stage, we choose a simple approach by overlaying two images. Specifically, we overlay the less distorted image on top of the more distorted one. This determination of distortion levels is guided by the UDIS++ registration method [Nie et al., 2023] and subsequent analysis, which identifies which of the two aligned images is more distorted. This initial overlay, while simple, typically results in visible seams in the image. To address this, we use an inpainting technique that focuses on the seam areas and uses a weighted mask to determine the amount of rendering required. It is important to note that our method does not rely on coarse rectangling in cases with minimal missing parts, as the initial overlap suffices. However, in situations with large missing areas, the presence of plain black inputs could disrupt the inpainting process. Thus, we implement coarse rectangling in advance to mitigate this issue and prepare the image for more effective inpainting.

3.3 Weighted Mask

We have adopted a large-scale diffusion model to perform the inpainting process within our image stitching framework. Recent studies, such as Repaint[Lugmayr et al., 2022], have shown that diffusion models excel in inpainting tasks and lead the field with their superior performance. This evidence strongly motivated our choice of this model.

In the diffusion models, the strength of inpainting is fundamentally affected by the intensity of the noise applied during the process. Recognizing this, we have developed an approach where the solution to both the fusion and rectangling challenges depends on the use of a carefully crafted weighted mask, $M_{guide}(x, y)$. This mask guides the denoising

steps of the diffusion process, effectively controlling the degree of inpainting to meet the specific requirements of the image regions being reconstructed.

First, we need to make the seam mask $M_{seam}(x, y)$ and the content mask $M_{content}(x, y)$. $M_{content}(x, y)$ is a very simple blend of $M_{wl}(x, y)$ and $M_{wr}(x, y)$, as shown below.

$$M_{content}(x, y) = M_{wl}(x, y) \vee M_{wr}(x, y) \quad (1)$$

$M_{seam}(x, y)$ is a bit more complicated to make, involving dilation, erosion, and some fusion operations, as shown below.

$$\begin{aligned} M_{seam}(x, y) &= M_{rseam}(x, y) \wedge M_{wr}(x, y) \\ M_{rseam}(x, y) &= (M_{dilation}(x, y) \oplus M_{wl}(x, y)) \vee (M_{erosion}(x, y) \oplus M_{wl}(x, y)) \\ M_{dilation}(x, y) &= (M_{wl} \oplus K)(x, y) = \max_{(i,j) \in K} \{M_{wl}(x+i, y+j)\} \\ M_{erosion}(x, y) &= (M_{wl} \ominus K)(x, y) = \min_{(i,j) \in K} \{M_{wl}(x+i, y+j)\} \end{aligned} \quad (2)$$

Where, \wedge , \vee , \oplus denote AND, OR, XOR. \oplus and \ominus denote dilation and erosion. And, K is the kernel size.

Then, we can make the weighted mask $M_{guide}(x, y)$ based on $M_{content}(x, y)$ and $M_{seam}(x, y)$, as shown below.

$$\begin{aligned} M_{guide}(x, y) &= M_{content}(x, y) \vee M_{gradient}(x, y) \\ M_{gradient}(x, y) &= (\neg M_{seam} \odot K)(x, y) = \min_{(i,j) \in K} \sqrt{(x-i)^2 + (y-j)^2} \end{aligned} \quad (3)$$

Where, \neg denotes NOR, and \odot is the distance transform.

We plot the weighted mask making process in Figure 3 to give a visualization.

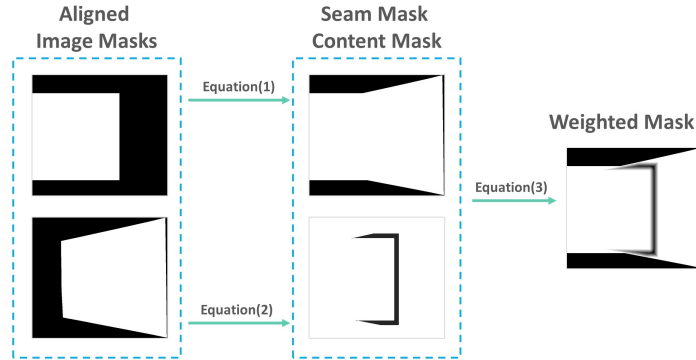


Figure 3: **Visual production process of weighted mask.** In the design of our weighted mask, we employ a grayscale scheme to visually represent the intensity of inpainting required for different areas of the image. In this scheme, different shades of gray indicate the degree of modification to be applied to the original content. Specifically, the white areas of the mask represent regions where no inpainting is applied, corresponding to an intensity level of 0. Conversely, the black areas indicate areas where inpainting should be applied at the highest intensity, denoted by an intensity level of 1. This gradation allows for precise control over the inpainting process, ensuring that changes are made appropriately to meet the needs of each specific area of the image.

3.4 Guided Denoising Inpainting

To effectively control the denoising process in the inpainting model, we incorporate the principles of Differential Diffusion[Levin and Fried, 2023] into the stable-diffusion-2-inpainting model[patrikvonplaten, 2023a], as shown in Figure 4. The input to this model includes the latent representations of the image, the mask, and the masked image.

During the initial phase of denoising, we start with an all-black mask. As the denoising process progresses, we gradually introduce the weighted mask into the equation. This gradual integration allows for precise modulation of the denoising intensity, ensuring that each area of the image receives the appropriate level of inpainting based on its specific needs.

The specific steps of the denoising process are detailed in Algorithm 1. The initial input to the algorithm is the coarse fusion and rectangling image, $I_{CFR}(x, y)$, which is derived using the following formula.

$$\begin{aligned}
 I_{CFR}(x, y) &= Telea(I_{CF}(x, y), M_{content}(x, y), R) \\
 I_{CF}(x, y) &= M_{overlap} \odot I_{wl}(x, y) + (1 - M_{overlap}) \odot I_{wr}(x, y) \\
 M_{overlap} &= M_{wl}(x, y) \wedge M_{wr}(x, y)
 \end{aligned} \tag{4}$$

Where, $Telea(\cdot)$ is the Alexandru Telea Algorithm[Telea, 2004], and R is the radius of a circular neighborhood of each point inpainted.

It is worth noting that our method does not require prompt guidance, while the previous stable diffusion inpaint models may generate many unwanted contents even if negative prompt guidance is added (the 7.3 provides more details), which is one of the advantages of our design.

Algorithm 1 Denoising Processing of SRStitcher

Input: Coarse Fusion and Rectangling Image $I_{CFR}(x, y)$, Weighted Mask $M_{guide}(x, y)$, Number of Steps N

Output: Fine Fusion and Rectangling Image $I_{FFR}(x, y)$

- 1: **INFERENCE**($I_{CFR}(x, y)$, $M_{guide}(x, y)$, N)
 - 2: prompt $p \leftarrow ""$ ▷ Our method does not require prompt guidance
 - 3: Init Mask $M_{init}(x, y) \leftarrow$ a black image with shape of $M_{guide}(x, y)$
 - 4: $Z_{init} \leftarrow LDM_Encoder(I_{CFR}(x, y))$
 - 5: $M_{ds}(x, y) \leftarrow Down_Sample(M_{guide}(x, y))$
 - 6: $Z'_N \leftarrow Add_Noise(Z_{init}, N)$
 - 7: $Z_{latent} \leftarrow Concat(Z'_N, M_{init}(x, y), Z_{init} \odot M_{init}(x, y))$
 - 8: $Z_N \leftarrow De_Noise(Z_{latent}, p, N)$
 - 9: **for** $t = N - 1$ to 0 **do**
 - 10: $Z'_t \leftarrow Add_Noise(Z_{t+1}, t)$
 - 11: $M_t(x, y) \leftarrow 1 - (M_{ds}(x, y) \preceq \frac{N-t}{N})$ ▷ \preceq means element-wise less-than
 - 12: $Z_{latent} \leftarrow Concat(Z'_t, M_t(x, y), Z_{init} \odot M_{init}(x, y))$ ▷ \odot means element-wise multiplication
 - 13: $Z_t \leftarrow De_Noise(Z_{latent}, p, t)$
 - 14: **end for**
 - 15: $I_{FFR}(x, y) \leftarrow LDM_Decoder(Z_0)$
-

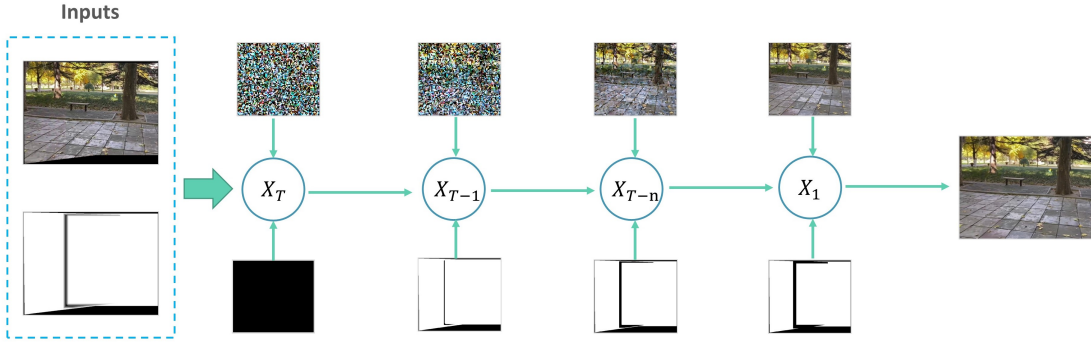


Figure 4: **Weighted mask guided denoising process.** During the denoising phase, we use weighted masks that undergo gradual changes to meticulously control the image denoising process. This approach allows us to precisely control the amount and intensity of inpainting applied to different areas of the image. Notably, our method achieves satisfactory results without relying on prompt guidance. By effectively using the dynamic adjustments in the weighted mask, our scheme ensures that the generated images meet high standards of quality and coherence, even in the absence of explicit prompts. This makes our method both efficient and effective, capable of handling complex image stitching scenarios independently.

4 Experiment

4.1 Experimental Setup

4.1.1 Dataset

To validate the performance of our proposed method, we conducted experiments on the large public dataset UDIS-D, originally introduced by UDIS[Nie et al., 2021]. Our procedure starts by aligning images with the registration network from UDIS++[Nie et al., 2023], followed by processing these aligned images through SRStitcher for both fusion and rectangling. All experiments described in this paper are based on these pre-aligned images.

4.1.2 Baselines

Our method is pioneering in integrating fusion and rectangling into a unified image stitching process. Given the novelty of this combination, no existing solutions simultaneously address all three stages of the image stitching pipeline as comprehensively as our method does (as detailed in the Statistics of Related Works 7.1 in the Supplemental Material). Consequently, we established our baselines by combining several existing solutions for comparative analysis.

Specifically, we employ publicly available models from UDIS[Nie et al., 2021] and UDIS++[Nie et al., 2023], which were pre-trained on the UDIS-D dataset, for tasks related to registration and fusion. For rectangling, we utilize models from DeepRectangling[Nie et al., 2022], as well as inpainting solutions like Lama[Suvorov et al., 2021] (Big-Lama), Stable-Diffusion-v1-5-inpainting[patrickvonplaten, 2023b], and Stable-Diffusion-v2-inpainting[patrickvonplaten, 2023a]. The details of these baseline configurations are presented in Table 1.

Table 1: Details of baselines

Name	Registration and Fusion	Rectangling
Baseline1	UDIS	DeepRectangling
Baseline2	UDIS++	DeepRectangling
Baseline3	UDIS	Lama
Baseline4	UDIS++	Lama
Baseline5	UDIS	Stable-Diffusion-v1-5-inpainting
Baseline6	UDIS++	Stable-Diffusion-v1-5-inpainting
Baseline7	UDIS	Stable-Diffusion-v2-inpainting
Baseline8	UDIS++	Stable-Diffusion-v2-inpainting

4.1.3 Metrics

Since UDIS-D is an unsupervised dataset, and to our knowledge, no supervised real-world datasets for deep learning-based image stitching currently exist, we are unable to employ Full-Reference Image Quality Assessment (FR-IQA) metrics. Attempting to artificially create ground truth for these images would be inherently subjective and could introduce bias, compromising the fairness of our evaluations.

Therefore, we chose to use No-Reference Image Quality Assessment (NR-IQA) metrics, which do not require a reference image for evaluation. This approach ensures a more objective assessment of image quality under the constraints of the UDIS-D dataset.

Specifically, we employ the following NR-IQA metrics:

- hyperIQA[Su et al., 2020]: an NR-IQA metric is designed for the wild image. hyperIQA is particularly suitable for the evaluation of the predominantly outdoor images in the UDIS-D dataset and therefore a suitable choice for our needs.
- CLIPQA[Wang et al., 2023]: an NR-IQA metric based on the Contrastive Language-Image Pre-training (CLIP) models, which allows for adaptable evaluations across different datasets. In our experiments, we use prompts such as ['nature image', 'stitched image'] to evaluate whether the stitched images appear more natural.

4.1.4 Implement Details

Our method is designed to operate without the need for model training or fine-tuning, ensuring simplicity and efficiency. All experiments were performed on a single NVIDIA 4090 GPU. In terms of specific settings for stable diffusion-based inference, we do not use prompts, the guidance scale is consistently set to 7.5, and the number of inference steps is fixed at 50.

In addition, the K value for $M_{seam}(x, y)$, which influences the seam correction, is set to 50. The K value for $M_{guide}(x, y)$, guiding the overall inpainting process, is set to 3. The R value for $I_{CR}(x, y)$, determining the rectangling effect, is set to 20.

4.2 Quantitative Evaluation

We performed a comprehensive quantitative analysis by comparing the results of 10,440 sample pairs from the UDIS-D training set and 1,106 sample pairs from the testing set. Notably, our method does not require training, so to provide a broader base of comparison, the training set of UDIS-D is also included in the comparison experiments. The results are detailed in Table 2, show that our method is the best performer.

However, upon closer examination of the test results, we found that the existing NR-IQA metrics did not perfectly capture the quality of the stitched images. In some cases, these metrics assigned high scores to images that visually appeared to be of poor quality (detailed in 7.4). This observation suggests that the real-world performance of our method may be even better than the current quantitative evaluation results indicate.

Table 2: Quantitative comparison on UDIS-D dataset [41]. The best is marked in bold.

Name	Testing Set		Training Set	
	hyperIQA↑	CLIPQA↑	hyperIQA↑	CLIPQA↑
Baseline1	42.53	0.28	45.31	0.31
Baseline2	45.98	0.31	49.87	0.33
Baseline3	42.55	0.27	45.63	0.30
Baseline4	46.57	0.31	51.28	0.33
Baseline5	43.26	0.25	48.65	0.28
Baseline6	46.43	0.27	51.20	0.30
Baseline7	42.60	0.28	47.36	0.34
Baseline8	46.96	0.31	51.92	0.34
Ours	47.64	0.35	54.26	0.39

4.3 Qualitative Evaluation

4.3.1 Verifying fault tolerance to registration errors

To evaluate the robustness of our method to registration inaccuracies, we selected several scenes from the UDIS-D dataset that present significant registration challenges. These examples are shown in Figure 5 and demonstrate the ability of our method to effectively handle complex registration scenarios.

The first scene contains wires, which are inherently difficult objects to register due to their elongated and thin structure, most registration methods struggle to accurately align such features; The second scene features a telephone pole positioned prominently in the foreground. Due to its central location, even minor registration errors are highly visible in the stitched output; The third scene contains an iron handrail with a complex shape and reflective surface, which complicates the alignment process. The interaction of light and metal surfaces adds an additional layer of difficulty to accurate registration; The fourth scene is characterized by repeated dense patterns, such as a large number of bricks. Such patterns pose significant challenges to existing registration methods, which often fail to accurately align repetitive textures.

4.3.2 Performance comparison of rectangling with extensive missing regions

The challenge of rectangling revolves around the quality and reliability of the inpainted image, especially when large regions are missing. Figure 6 provides the inpainting results of different methods with extensive missing regions.

Experimental results show that mesh-based methods (baseline1 and baseline2) are completely inadequate for dealing with scenes with significant missing areas. These methods typically fail to reconstruct meaningful or coherent image content under such challenging conditions.

In addition, the performance of other inpainting-based methods (baseline3-8) also proves unsatisfactory in scenarios with large missing regions. These methods often resort to generating odd patterns or simply choosing similar colors to fill the gaps. Unfortunately, this approach generally fails to recreate precise structural and textural details, resulting in an inpainted image that lacks visual coherence and authenticity.

4.4 User Study

Considering the limitations of quality evaluation metrics, we introduce a user study metric approach similar to the experimental schemes used in UDIS and UDIS++. This method allows for a more subjective but insightful assessment of visual quality through direct user feedback.

For the user study, we display four images simultaneously on a single screen: the two input images, our stitched result, and the stitched result from one of the baseline methods. Participants are given the opportunity to zoom in on the images for detailed examination and are asked to determine which result is superior. In cases where a clear preference is not apparent, participants are asked to classify the results as either "both good" or "both bad," adding further granularity to the feedback.

The study involves 20 participants, evenly split between those with a background in computer vision (researchers and students) and those without a computer-related major (general volunteers). This diverse group ensures a balanced perspective, combining expert technical evaluation with general user impressions. The results of the user study are shown in Figure 7.

4.5 Ablation Study

Due to the limitations of quantitative metrics, which often fail to capture subtle improvements and optimizations in image quality. We continue to use a qualitative evaluation approach in the ablation study. This approach provides a more nuanced understanding of how different parameters affect the performance of our method. As shown in Figure 8, this approach allows us to visually assess the impact of various adjustments, allowing for a direct comparison of the effects that specific parameter changes have on the final stitched images.

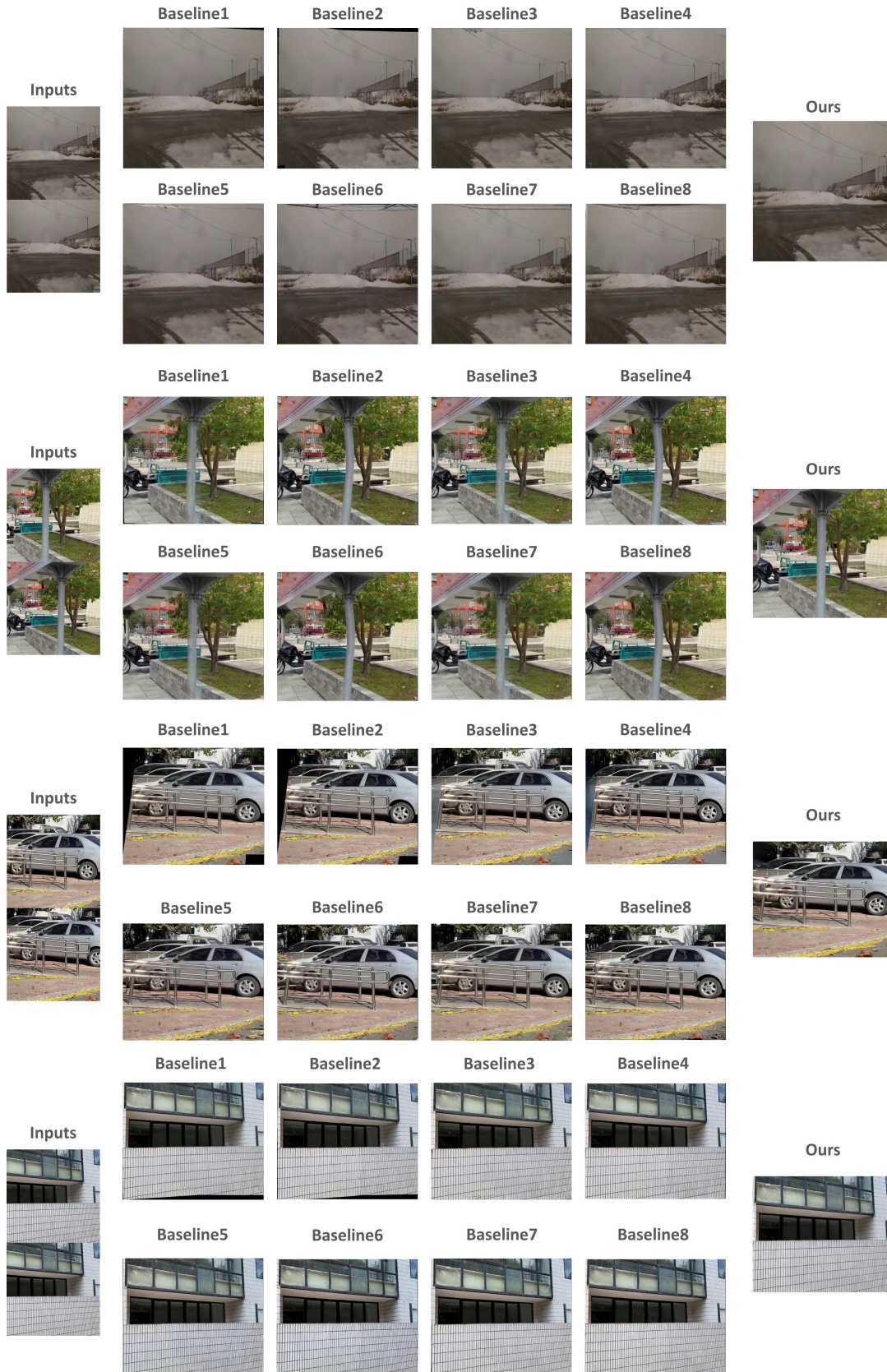


Figure 5: **Comparison of visualization results with registration errors.** We selected several scenarios with registration error challenges.

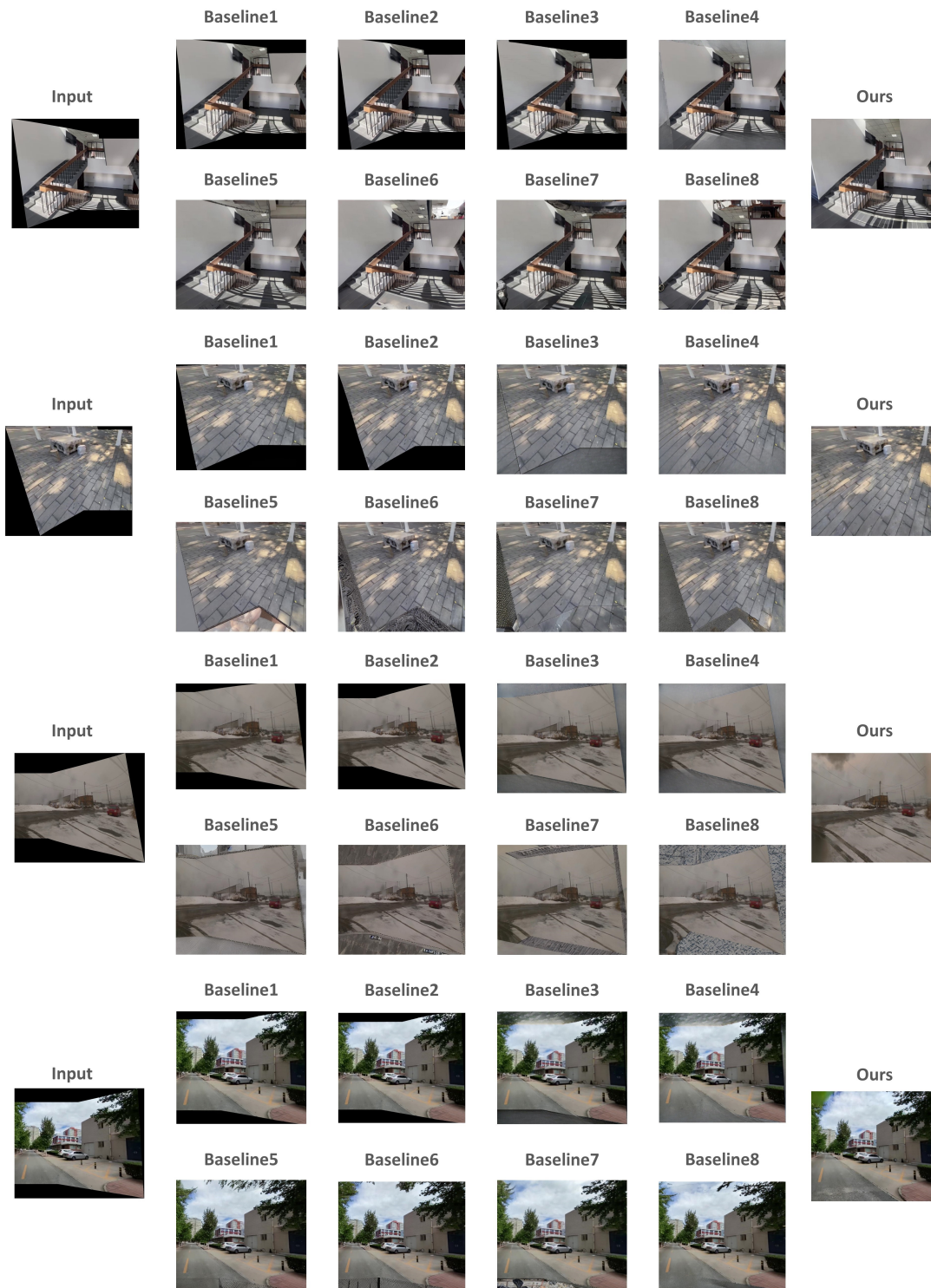


Figure 6: **Comparison of visualization results with a large number of missing regions.** For the sake of simplicity, we have chosen only the UIDS++ fusion image as 'input'. In fact, the inputs of the different methods are different, but the missing rectangular areas are the same.

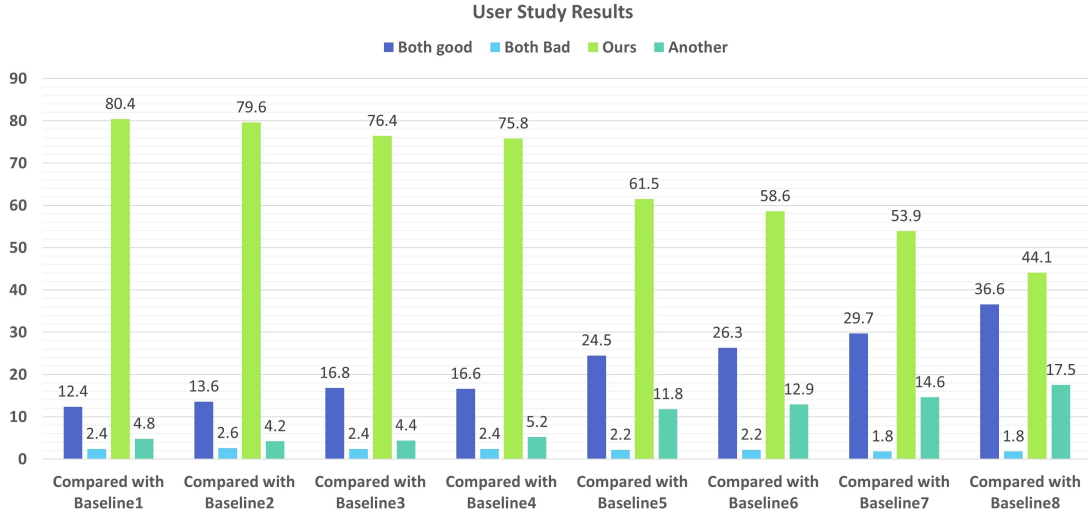


Figure 7: **User study on visual quality.** The numbers are shown in percentage and averaged on 20 participants.

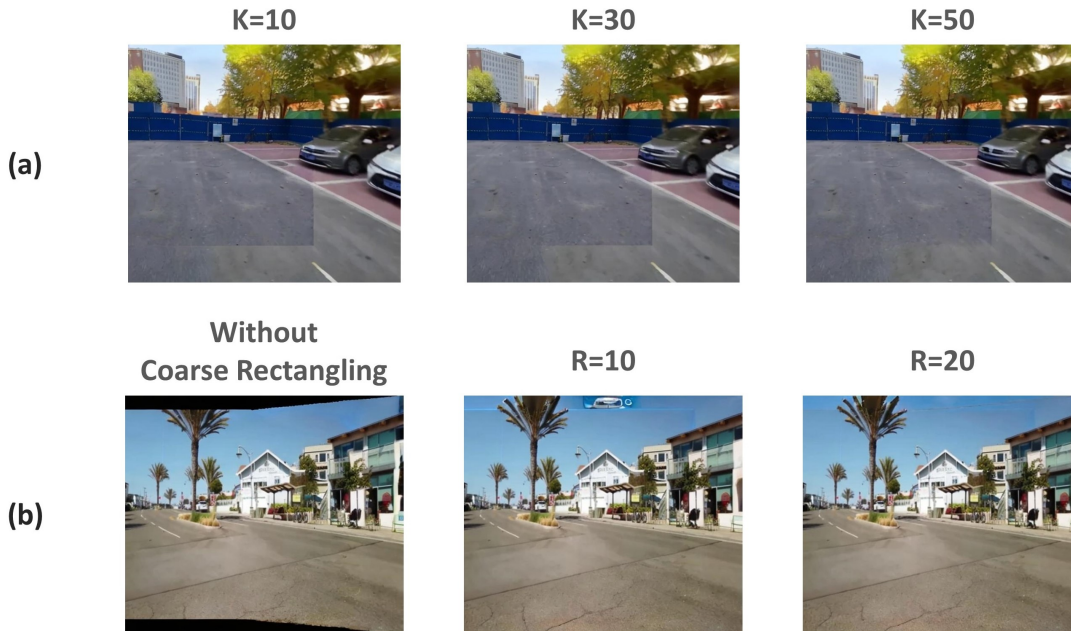


Figure 8: **Ablation study.** (a) Effect of K in $M_{seam}(x, y)$ on visual performance. The parameter K plays a crucial role in determining the amount of modification along the seam of stitched images. A lower value of K can result in unnatural and excessive changes, making the seam prominently visible and disrupting image continuity. Conversely, a higher value of K increases the modification area around the seam, potentially affecting more of the image than necessary. This setting must be finely tuned to ensure seamless integration without overextending the modifications. (b) Effect of R in $I_{CR}(x, y)$ on visual performance. The R parameter affects the effectiveness of the coarse rectangling process, especially when dealing with large missing regions. Without implementing coarse rectangling, our method struggles with large missing regions, often resulting in prominent black backgrounds. Introducing coarse rectangling with an appropriate R value helps to produce more finely filled images, thereby improving the visual quality of the final output. However, it's important to note that higher values of R not only improve image fill quality, but also slow down the image preprocessing phase. This trade-off between image quality and processing speed must be considered in order to optimize the performance of our stitching method.

5 Limitation and Future work

Despite the demonstrated effectiveness of our proposed method, there are several limitations that warrant further investigation:

- (1) **Handling of Large Missing Regions:** Our method occasionally produces local blur in the results when dealing with rectangles with large missing areas. Currently, we have not found an effective way to consistently convert blur results into sharp images. This problem may be due to relying solely on a pre-trained model, which has its limitations despite its robust generalization capabilities. Slight fine-tuning of the model could potentially improve its performance.
- (2) **Color Discrepancy Issues:** When input images have significant color differences, our method tends to leave visible seams. While adjusting the K value provides some improvement, it does not completely solve the problem in all scenarios. Integrating additional image pre-processing techniques to specifically address color discrepancies prior to stitching could further improve the consistency of the results.
- (3) **Content Anomalies:** Our method does not use prompts, which generally gives good results. However, there remains a small probability of generating unwanted content, such as strange text or patterns. Future work could explore the incorporation of more sophisticated guidance methods to refine content generation and minimize the occurrence of these anomalies.

6 Conclusion

This paper presents a novel design for the image stitching pipeline that redefines the fusion and rectangling stages as unified inpainting tasks that are addressed simultaneously using a single inference model. The proposed method uses a weighted mask to guide different levels of the denoising process, allowing for differentiated inpainting intensities across the stitched image. This technique achieves high-quality stitching without the need for additional model training, demonstrating increased tolerance for registration errors and improving the overall content integrity of the stitched images. However, this method faces challenges in dealing with scenes with large missing areas, handling color discrepancies between input images, and the occasional appearance of unwanted content. Future work will focus on addressing these issues in order to refine and extend the applicability of our stitching method.

References

- Lang Nie, Chunyu Lin, Kang Liao, Shuaicheng Liu, and Yao Zhao. Unsupervised deep image stitching: Reconstructing stitched features to images. *IEEE Transactions on Image Processing*, 30:6184–6197, 2021. ISSN 1941-0042. doi:10.1109/tip.2021.3092828. URL <http://dx.doi.org/10.1109/TIP.2021.3092828>.
- Senmao Cheng, Fan Yang, Zhi Chen, Nanjun Yuan, and Wenbing Tao. Deep seam prediction for image stitching based on selection consistency loss. *arXiv preprint arXiv:2302.05027*, 2023.
- Lang Nie, Chunyu Lin, Kang Liao, Shuaicheng Liu, and Yao Zhao. Deep rectangling for image stitching: a learning baseline. In *Proceedings of the IEEE/CVF conference on computer vision and pattern recognition*, pages 5740–5748, 2022.
- Lang Nie, Chunyu Lin, Kang Liao, and Yao Zhao. Learning edge-preserved image stitching from large-baseline deep homography, 2020a.
- Lang Nie, Chunyu Lin, Kang Liao, Shuaicheng Liu, and Yao Zhao. Parallax-tolerant unsupervised deep image stitching. In *Proceedings of the IEEE/CVF International Conference on Computer Vision*, pages 7399–7408, 2023.
- Imad Zoghlami, Olivier Faugeras, and Rachid Deriche. Using geometric corners to build a 2d mosaic from a set of images. In *Proceedings of IEEE computer society conference on computer vision and pattern recognition*, pages 420–425. IEEE, 1997.
- David Capel and Andrew Zisserman. Automated mosaicing with super-resolution zoom. In *Proceedings. 1998 IEEE Computer Society Conference on Computer Vision and Pattern Recognition (Cat. No. 98CB36231)*, pages 885–891. IEEE, 1998.
- Philip F McLauchlan and Allan Jaenicke. Image mosaicing using sequential bundle adjustment. *Image and Vision computing*, 20(9-10):751–759, 2002.
- Matthew Brown and David G Lowe. Automatic panoramic image stitching using invariant features. *International journal of computer vision*, 74:59–73, 2007.
- Junhong Gao, Seon Joo Kim, and Michael S Brown. Constructing image panoramas using dual-homography warping. In *CVPR 2011*, pages 49–56. IEEE, 2011.

- Tianli Liao and Nan Li. Natural image stitching using depth maps, 2023.
- Jian Yu, Yi Yu, and Feipeng Da. Parallax-tolerant image stitching with epipolar displacement field, 2023.
- Van-Dung Hoang, Diem-Phuc Tran, Nguyen Gia Nhu, The-Anh Pham, and Van-Huy Pham. Deep feature extraction for panoramic image stitching. In *Intelligent Information and Database Systems: 12th Asian Conference, ACIIDS 2020, Phuket, Thailand, March 23–26, 2020, Proceedings, Part II 12*, pages 141–151. Springer, 2020.
- Zaifeng Shi, Hui Li, Qingjie Cao, Huizheng Ren, and Boyu Fan. An image mosaic method based on convolutional neural network semantic features extraction. *Journal of Signal Processing Systems*, 92:435–444, 2020.
- Lang Nie, Chunyu Lin, Kang Liao, Meiqin Liu, and Yao Zhao. A view-free image stitching network based on global homography. *Journal of Visual Communication and Image Representation*, 73:102950, 2020b.
- Mingbo Hong, Yuhang Lu, Nianjin Ye, Chunyu Lin, Qijun Zhao, and Shuaicheng Liu. Unsupervised homography estimation with coplanarity-aware gan. In *Proceedings of the IEEE/CVF Conference on Computer Vision and Pattern Recognition (CVPR)*, pages 17663–17672, June 2022.
- Zhiying Jiang, Zengxi Zhang, Jinyuan Liu, Xin Fan, and Risheng Liu. Multi-spectral image stitching via spatial graph reasoning. In *Proceedings of the 31st ACM International Conference on Multimedia*, pages 472–480, 2023a.
- Hai Jiang, Haipeng Li, Yuhang Lu, Songchen Han, and Shuaicheng Liu. Semi-supervised deep large-baseline homography estimation with progressive equivalence constraint. In *Proceedings of the AAAI Conference on Artificial Intelligence*, volume 37, pages 1024–1032, 2023b.
- Si-Yuan Cao, Runmin Zhang, Lun Luo, Beinan Yu, Zehua Sheng, Junwei Li, and Hui-Liang Shen. Recurrent homography estimation using homography-guided image warping and focus transformer. In *Proceedings of the IEEE/CVF Conference on Computer Vision and Pattern Recognition (CVPR)*, pages 9833–9842, June 2023.
- Alex M Andrew. Multiple view geometry in computer vision. *Kybernetes*, 30(9/10):1333–1341, 2001.
- Julio Zaragoza, Tat-Jun Chin, Michael S Brown, and David Suter. As-projective-as-possible image stitching with moving dlt. In *Proceedings of the IEEE conference on computer vision and pattern recognition*, pages 2339–2346, 2013.
- Aseem Agarwala, Mira Dontcheva, Maneesh Agrawala, Steven Drucker, Alex Colburn, Brian Curless, David Salesin, and Michael Cohen. Interactive digital photomontage. In *ACM SIGGRAPH 2004 Papers*, pages 294–302. 2004.
- Junhong Gao, Yu Li, Tat-Jun Chin, and Michael S Brown. Seam-driven image stitching. In *Eurographics (Short Papers)*, pages 45–48, 2013.
- Kaimo Lin, Nianjuan Jiang, Loong-Fah Cheong, Minh Do, and Jiangbo Lu. Seagull: Seam-guided local alignment for parallax-tolerant image stitching. In *Computer Vision—ECCV 2016: 14th European Conference, Amsterdam, The Netherlands, October 11–14, 2016, Proceedings, Part III 14*, pages 370–385. Springer, 2016.
- Kaiming He, Huiwen Chang, and Jian Sun. Rectangling panoramic images via warping. *ACM Transactions on Graphics (TOG)*, 32(4):1–10, 2013.
- Dongping Li, Kaiming He, Jian Sun, and Kun Zhou. A geodesic-preserving method for image warping. In *Proceedings of the IEEE Conference on Computer Vision and Pattern Recognition*, pages 213–221, 2015.
- Tianhao Zhou, Haipeng Li, Ziyi Wang, Ao Luo, Chen-Lin Zhang, Jiajun Li, Bing Zeng, and Shuaicheng Liu. Recdiffusion: Rectangling for image stitching with diffusion models, 2024.
- Prune Truong, Martin Danelljan, and Radu Timofte. Glu-net: Global-local universal network for dense flow and correspondences. In *Proceedings of the IEEE/CVF conference on computer vision and pattern recognition*, pages 6258–6268, 2020.
- Andreas Lugmayr, Martin Danelljan, Andres Romero, Fisher Yu, Radu Timofte, and Luc Van Gool. Repaint: Inpainting using denoising diffusion probabilistic models, 2022.
- Eran Levin and Ohad Fried. Differential diffusion: Giving each pixel its strength, 2023.
- patrickvonplaten. stable-diffusion-2-inpainting. <https://huggingface.co/stabilityai/stable-diffusion-2-inpainting>, 2023a.
- Alexandru Telea. An image inpainting technique based on the fast marching method. *Journal of graphics tools*, 9(1): 23–34, 2004.
- Roman Suvorov, Elizaveta Logacheva, Anton Mashikhin, Anastasia Remizova, Arsenii Ashukha, Aleksei Silvestrov, Naejin Kong, Harshith Goka, Kiwoong Park, and Victor Lempitsky. Resolution-robust large mask inpainting with fourier convolutions. *arXiv preprint arXiv:2109.07161*, 2021.

- patrickvonplaten. stable-diffusion-2-inpainting. <https://huggingface.co/runwayml/stable-diffusion-inpainting/blob/main/sd-v1-5-inpainting.ckpt>, 2023b.
- Shaolin Su, Qingsen Yan, Yu Zhu, Cheng Zhang, Xin Ge, Jinqiu Sun, and Yanning Zhang. Blindly assess image quality in the wild guided by a self-adaptive hyper network. In *IEEE/CVF Conference on Computer Vision and Pattern Recognition (CVPR)*, June 2020.
- Jianyi Wang, Kelvin CK Chan, and Chen Change Loy. Exploring clip for assessing the look and feel of images. In *AAAI*, 2023.
- liudakai2. Unsupdis-pytorch, 2022. URL <https://github.com/liudakai2/UnsupDIS-pytorch>.
- Alex and McKinney. Image to image inpainting stable diffusion. <https://github.com/huggingface/diffusers/tree/08bf7545070764d41637e90290ca9b92b392263e/examples/community#image-to-image-inpainting-stable-diffusion>, 2022.

7 Supplemental Material

In this document, we provide the following supplementary contents:

- Statistics of related works.
- Mathematical analysis of the fusion problem and the rectangling problem.
- Comparison of the effect of our method and the other stable diffusion inpaint model without prompt.
- Limitaitons of NR-IQA metrics.
- How to modify our method without using coarse rectangling.

7.1 Statistics of related works

In our comprehensive review of recent deep learning-based image stitching research(as shown in Table 3), we identified a gap in the existing literature: no previous work has addressed the tasks of fusion and rectangling within a single unified model. Our study is the first to propose such an integrated method. This novelty not only simplifies the stitching process by reducing the complexity of transitioning between separate stages, but also increases the efficiency and effectiveness of the output.

Table 3: Statistics for the deep image stitching related works

Work	Registration	Fusion	Rectangling
VFISNet [Nie et al., 2020b]	✓	✓	✗
EPISNet [Nie et al., 2020a]	✓	✓	✗
UDIS [Nie et al., 2021]	✓	✓	✗
UDIS-Variant [liudakai2, 2022]	✓	✓	✗
UDIS++ [Nie et al., 2023]	✓	✓	✗
Dseam Cheng et al. [2023]	✗	✓	✗
Jiang et al. [Jiang et al., 2023a]	✓	✓	✗
LBHomo [Jiang et al., 2023b]	✓	✗	✗
RHWF [Cao et al., 2023]	✓	✗	✗
HomoGAN [Hong et al., 2022]	✓	✗	✗
DeepRectangling [Nie et al., 2022]	✗	✗	✓
RecDiffusion [Zhou et al., 2024]	✗	✗	✓
SRStitcher(Ours)	✓	✓	✓

7.2 Mathematical analysis of the fusion problem and the rectangling problem

Suppose an image can be represented as $I(x, y)$, where x and y are spatial coordinates.

7.2.1 Fusion problem

The fusion problem is essentially a local pixel modification problem to an image, which can be defined as:

Given an image $I(x, y)$ and a mask $M(x, y)$, the mask defines the area of the image that needs to be modified. We want to change the pixel value of the mask region from $I(x, y)$ to a new pixel value $I'(x, y)$ via the function $V(\cdot)$. Mathematically, this can be expressed as follows.

$$I'(x, y) = I(x, y) \odot (1 - M(x, y)) + V(I(x, y)) \odot M(x, y) \quad (5)$$

7.2.2 Rectangling problem

The rectangling problem is essentially a local pixel filling problem to an image, which can be defined as:

Given an image $I(x, y)$ and a mask $M(x, y)$, the mask defines the area of the image that needs to be filled. We want to change the pixel value of the mask region from $I(x, y)$ to a new pixel value $I'(x, y)$ via the function $G(\cdot)$. Mathematically, this can be expressed as follows.

$$I'(x, y) = I(x, y) \odot (1 - M(x, y)) + G(I(x, y)) \odot M(x, y) \quad (6)$$

From the above mathematical expression, we can see that whether it is local modification or local filling, we are operating on the masked regions of the image and keeping the pixel values in the non-masked regions unchanged. So what we need to do is to find a model that achieves both $V(\cdot)$ and $G(\cdot)$.

In the diffusion model, $V(\cdot)$ and $G(\cdot)$ are unified as a denoising function $Denoise(\cdot)$ [Alex and McKinney, 2022], the above two formulas can be unified into:

$$I'(x, y) = Denoise(I(x, y), M(x, y), P(x, y)) \quad (7)$$

Where, $P(x, y)$ is guidance for the denoising. In this paper, we use weighted mask to implement the function of $P(x, y)$.

7.3 Comparison of the effect of our method and the other stable diffusion inpaint model without prompt

We conducted a comparative study of our method against Stable-Diffusion-v1-5-inpainting (SD1.5)[patrickvonplaten, 2023b] and Stable-Diffusion-v2-inpainting (SD2)[patrickvonplaten, 2023a], using the same settings for non-prompt and random seed. The visual results of this comparison are shown in Figure 9. Our results indicate that current stable diffusion inpainting models are susceptible to biases from their training data, which can lead to the generation of unwanted artifacts such as strange text and abrupt patterns, particularly noticeable in night scenes. Our method significantly mitigates these issues, demonstrating a marked improvement in maintaining the consistency and relevance of the inpainting content.

7.4 Limitations of NR-IQA metrics

By analysis of the results obtained using two No-Reference Image Quality Assessment (NR-IQA) metrics, hyperIQA and CLIPQA, we find that these metrics may not accurately capture human sensory preferences for image quality. Although our method produces higher quality and more authentic images, as visually demonstrated in Figure 10, the corresponding scores awarded by these metrics are relatively low.

This discrepancy suggests that hyperIQA and CLIPQA may have inherent flaws when applied to the evaluation of stitched image quality. The metrics appear to fall short in recognizing and quantifying the nuanced aspects of image authenticity and overall visual appeal that are perceptible to human observers. Therefore, we assert that there is a need for a user study.

7.5 How to modify our method without using coarse rectangling

Our solution only needs minor modifications to produce decent results without need of coarse rectangling. Specifically, our method can be modified by replacing the all-black initialization mask $M_{init}(x, y)$ in Algorithm 1 with the reverse content mask $\neg M_{content}(x, y)$. This modification helps to avoid the black color interference in the image background during inpainting.

However, this method has shown a tendency to produce results similar to those of baselines 5-8, where the lack of prompt guidance can lead to the appearance of unwanted objects in the inpainted images. Thus, despite the potential of this approach to simplify the process, it was observed that it could compromise the stability of the final output.

Based on these findings, we continue to recommend the coarse-to-fine method outlined in the paper. This approach not only maintains the quality of the generated images, but also ensures greater consistency and reliability in the inpainting effects.



Figure 9: The comparison of the results of inpainting images without prompt guidance proves that our method has a lower probability of generating abnormal content.



Figure 10: The comparison of the results of NR-IQA metrics.